Guaranteed-accuracy quantum annealing

Takashi Imoto,[1] Yuya Seki,[1] Yuichiro Matsuzaki,[1,2,*] and Shiro Kawabata[1,2,†]

[1]*Research Center for Emerging Computing Technologies (RCECT), National Institute of Advanced Industrial Science and Technology (AIST), 1-1-1 Umezono, Tsukuba, Ibaraki 305-8568, Japan*

[2]*NEC-AIST Quantum Technology Cooperative Research Laboratory, National Institute of Advanced Industrial Science and Technology (AIST), Tsukuba, Ibaraki 305-8568, Japan*

(Received 13 March 2021; accepted 6 July 2022; published 28 October 2022)

Quantum chemistry calculations constitute an important application of quantum annealing (QA). For practical applications in quantum chemistry, it is essential to estimate the ground-state energy of the Hamiltonian with chemical accuracy. However, there is no known method for guaranteeing the accuracy of the energy estimated via QA. Here, we propose a method for guaranteeing the accuracy of the energy estimated via QA using the Weinstein and Temple bounds. In our scheme, before QA is performed, the energies of the ground state and first excited state must be preestimated with some error bars (corresponding to the possible estimation error) via classical computation with some approximations. We show that, if the expectation value and standard deviation of the energy of the state after QA are lower than certain threshold values (that we can calculate from the preestimation), the ground-state energy estimated by QA is closer to the ground-state energy than the preestimation. As the expectation value and standard deviation of the energy can be experimentally measured via QA, our results pave the way for accurate estimation of the ground-state energy using QA.

DOI: 10.1103/PhysRevA.106.042615

I. INTRODUCTION

In recent years, quantum chemistry calculations have attracted considerable attention as a novel application of quantum devices because of their potential use in medical fields. One of the main purposes of quantum chemistry is to calculate the energy of the molecular Hamiltonian. High accuracy of the energy of chemical materials is required, i.e., at least 1.6×10^{-3} hartree, where 1 hartree $= e^2/4\pi\epsilon_0 a_0 =$ 27.211 eV and $a_0 = 1$ bohr $= 0.529 \times 10^{-10}$ m. This accuracy is called chemical accuracy. Energy with chemical accuracy allows us to estimate the chemical reaction rate at room temperature using the Eyring equation [1].

There are sophisticated techniques for mapping the molecular Hamiltonian with the second quantized form into a spin Hamiltonian. These techniques are important for implementing quantum chemistry calculations using quantum devices composed of qubits, because the Hamiltonian for describing the molecules in the quantum devices should be written using the Pauli matrices. We can map the second-quantized many-body Hamiltonians onto those of qubit systems using the Bravyi–Kitaev transformation [2–6]. In addition, there are ways to generate effective three-body interactions using two-body interactions [7,8].

There is an improvement over the Jordan–Wigner transformation in terms of the required number of qubit operators per fermionic operator. The Jordan–Wigner transformation maps one of n fermionic operators to $O(n)$ qubit operators. By contrast, the Bravyi–Kitaev transformation maps one of n fermionic operators to $O(\log(n))$ qubits. A comparison between the gate numbers of the Bravyi–Kitaev and Jordan–Wigner transformations to obtain the ground state and the lowest energy with the Trotter decomposition has been reported [9]. Furthermore, Babbush *et al.* represented the Hamiltonian using only a two-local interaction between spins [10].

Quantum algorithms have also been proposed for fault-tolerant quantum computation in quantum chemistry calculations [11–13]. In addition, molecular energies have been obtained using phase-estimation algorithms [14,15]. However, a fault-tolerant quantum computer requires many qubits with high-fidelity gate operations beyond the capability of a near-term quantum computer to perform error correction. Therefore, algorithms for quantum chemistry have not been experimentally implemented with a practically useful size thus far.

Recently, noisy intermediate-scale quantum (NISQ) computing has been proposed [16–18]. A promising algorithm for NISQ is the variational quantum eigensolver (VQE) with the variational method [19,20]. The VQE gives the lowest eigenvalue of a Hamiltonian, such as that of a chemical material. It is a hybrid quantum-classical algorithm. Variational algorithms have also been used to simulate quantum dynamics [21,22]. The standard deviation has been used to determine how close the quantum state is to the energy eigenstate in the NISQ algorithm [23].

Quantum annealing (QA) is also a promising method for implementing quantum chemistry calculations. It has traditionally been used to solve combinatorial optimization problems [24,25]. We map a combinatorial optimization prob-

*matsuzaki.yuichiro@aist.go.jp
†s-kawabata@aist.go.jp

lem into the Ising Hamiltonian H_P and we call this a problem Hamiltonian whose ground state corresponds to the solution of the combinatorial optimization problem. Meanwhile, we use another Hamiltonian H_D that represents transverse magnetic fields, which we call a driver Hamiltonian. In QA, we prepare a ground state of H_D and the total time-dependent Hamiltonian is changed from H_D to H_P within an annealing time T. As long as then the adiabatic condition is satisfied, the adiabatic theorem guarantees that the ground state of the problem Hamiltonian can be obtained via QA. Importantly, by replacing H_P with the molecular Hamiltonian, QA can be used to estimate the energy of the ground state in quantum chemistry [6,26–29]. In addition, the search for excited states in quantum chemistry has been discussed [30,31].

D-Wave Systems Inc. [32] realized QA machines composed of thousands of qubits. They used superconducting flux qubits to implement QA. There have been many experimental demonstrations of QA using the devices of D-Wave Systems Inc. [33–36]. In particular, quantum chemistry calculations have been demonstrated using QA to estimate the ground-state energy for a small-sized molecule [28]. Also, recently, a coupler to realize a no-stoquastic Hamiltonian was developed and there were some experimental demonstrations for this [37,38]. It is worth mentioning that the coherence time of the qubits with the D-wave machine is less than 100 ns [39] and this short coherence time makes it difficult to realize single qubit operations except computational basis measurements. On the other hand, by using a recently proposed scheme called a spin-lock QA, it is possible to use long-lived qubits such, as capacitively shunted flux qubits, and we can perform arbitrary single qubit operations in this architecture (see Appendix D) [40,41].

The potential problem in using QA for practical quantum chemistry calculations arises because of the intrinsic error in QA. Nonadiabatic transitions induce a transition from the ground state to excited states. Moreover, decoherence owing to the coupling with the environment causes unwanted decay of the quantum states during QA. Because of these problems, it is not clear whether chemical accuracy can be achieved in quantum chemistry calculations using QA. Therefore, it is essential to achieve higher accuracy to estimate the ground-state energy in QA.

In this paper, we propose a method for estimating the energy of the target Hamiltonian with guaranteed accuracy, where we combine QA with classical computation. The energy calculated from QA should be larger than the true ground-state energy owing to errors and the difference between the energy calculated from QA and the true energy is defined as the estimation error. The upper bound of such an estimation error is called an error bar. To measure the error bar, we use the Weinstein bound: if the population of the ground state is more than $1/2$ after QA, the standard deviation of the energy (that we can experimentally measure) provides us with the upper bound of the estimation error. We present a method for checking whether the population of the ground state is more than $1/2$ after QA by using classical computation. We must determine the possible range of the energies of the ground state and first excited state before QA by performing classical computation with some approximation (such as a mean-field technique). We can calculate a certain threshold

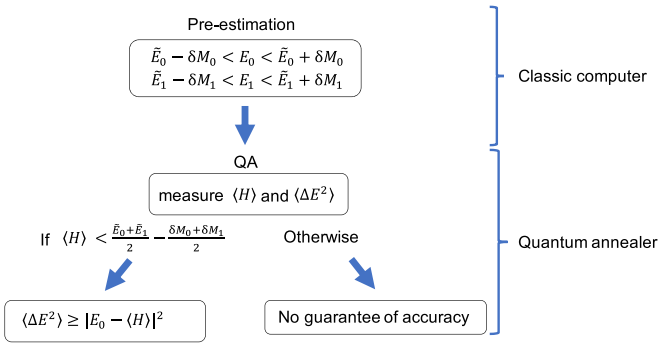

FIG. 1. Flow chart showing how to estimate the ground-state energy of the target Hamiltonian in our protocol. We must preestimate the ground-state energy using a classical computer with some approximation and determine $\tilde{E}_0$, $\tilde{E}_1$, δM_0, and δM_1, where $\tilde{E}_0$ ($\tilde{E}_1$) is the approximated ground (first-excited) -state energy from the preestimation and δM_0 (δM_1) is the error bound of the preestimation. In addition, E_0 (E_1) denotes the true energy of the ground (first excited) state and $\langle H\rangle$ ($\langle \Delta E^2\rangle$) denotes the expectation (the squared standard deviation) of the Hamiltonian of the state after QA. In our protocol, when $\langle H\rangle$ is smaller than $(\frac{\tilde{E}_1-\tilde{E}_0}{2} - \frac{\delta M_0+\delta M_1}{2})$, the standard deviation of the state after QA can be the upper bound of the estimation error.

by using values from the preestimation and, if the energy estimated by QA is lower than the threshold, the population of the ground state is more than $1/2$ after QA. In addition, if the classical error bars (corresponding to the possible estimation error) given by the preestimation are larger than the standard deviation of the energy measured from QA, we can use the standard deviation of the energy as the improved error bars for the energy estimation. The method is schematically shown in Fig. 1. Moreover, in order to reduce the error, we employ the Temple bound. To do that, we must determine the lower bound of the energy of the first excited state via classical computation. If the ground-state energy estimated with QA is smaller than the bound, we can obtain the error bar of the estimation. This method is schematically shown in Fig. 2.

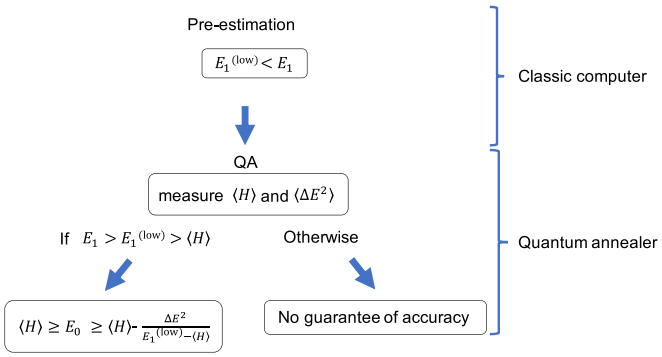

FIG. 2. Flow chart showing how to estimate the ground-state energy of the target Hamiltonian in our protocol using the Temple bound. We must preestimate the lower bound $E_1^{(\mathrm{low})}$ of the first-excited-state energy using a classical computer. When the energy from QA satisfies $E_1^{(\mathrm{low})} > \langle H\rangle$, we obtain the lower bound of the ground-state energy E_0, $\langle H\rangle - \frac{\Delta E^2}{E_1^{(\mathrm{low})} - \langle H\rangle}$. Here, we use the same notation as that in Fig. 1.

We numerically demonstrate that this approach provides more accurate error bars than the approach based on the Weinstein bound. It is worth mentioning that, although we focus on QA as a primary application of our method, our scheme is also useful for the other schemes to find a ground state such as a variational quantum eigensolver with NISQ devices [19].

The remainder of this paper is organized as follows. Section II reviews QA. Section III introduces the Weinstein and Temple bounds. Section IV describes our approach of using the Weinstein and Temple bounds for obtaining the error bars for the energy estimation with QA.

Section V describes our method for estimating the ground-state energy of the hydrogen molecule to evaluate the performance of our scheme. Finally, Sec. VI summarizes our findings.

II. QUANTUM ANNEALING

Here, we review QA for the ground-state search. We regard the driving Hamiltonian as the transverse field. The total Hamiltonian for QA is described as follows:

$$H(t) = \frac{t}{T}H_P + \left(1 - \frac{t}{T}\right)H_D, \tag{1}$$

where T is the annealing time. First, we prepare the ground state of the transverse field $H_D = -\sum_{i=1}^{N} \hat{\sigma}_i^x$, $|\Psi(0)\rangle = |+\cdots+\rangle$, where the quantum state $|+\rangle$ denotes the eigenstate of σ^x with the eigenvalue $+1$. Second, the driver Hamiltonian is adiabatically changed into the problem Hamiltonian. Finally, we obtain the ground state of the problem Hamiltonian if the dynamics is adiabatic; hence the measurement of an observable H_P provides the ground-state energy.

Various forms of noise degrade the accuracy of QA. The main sources of such noise are environmental decoherence and nonadiabatic transitions. There is a trade-off between these two errors. We should implement QA slowly to avoid nonadiabatic transitions; however, slow dynamics tends to increase the error owing to decoherence.

Many attempts have been made to suppress nonadiabatic transitions and decoherence. To find a ground state of the Ising Hamiltonian, the use of nonstoquastic Hamiltonians has been proposed to increase the energy gap during QA for a specific model, which could contribute toward the suppression of nonadiabatic transitions [42–45]. An inhomogeneous driving Hamiltonian for a p-spin model is known to contribute toward accelerating QA for specific cases [46,47]. It is shown that the use of Ramsey type measurements can suppress the degradation due to the nonadiabatic transitions in QA [25]. Both theoretical and experimental studies have been conducted to suppress decoherence during QA. Error correction techniques [48], spin lock techniques [40,49,50], and decoherence-free subspaces [51,52] can be used for the suppression of decoherence. In addition, a method involving nonadiabatic transition and quenching for efficient QA has also been investigated [53–60]. Counterdiabatic driving is considered as one of the approaches to improve the performance of the QA [61–67].

Despite previous efforts, there is no universal way to suppress both environmental decoherence and nonadiabatic transitions during QA, which makes it difficult to guarantee the accuracy of the results of QA.

III. WEINSTEIN BOUND AND TEMPLE BOUND

Here, we review the Weinstein and Temple bounds. Let E_0 (E_1) denote the true energy of the ground (first excited) state. First, we introduce the Weinstein bound [68].

Theorem 1. If the state $\langle\psi|$ satisfies $\langle\psi|\psi_0\rangle \geqslant \frac{1}{2}$, then we obtain

$$\sigma \geqslant \langle\psi|H|\psi\rangle - E_0, \tag{2}$$

where $\sigma = \sqrt{\langle\psi|H^2|\psi\rangle - \langle\psi|H|\psi\rangle^2}$ denotes the standard deviation of the energy and $|\psi_0\rangle$ is the true ground state.

Next, we introduce the Temple bound [69].

Theorem 2. If we know the exact first excited energy E_1 and a state $|\psi\rangle$ satisfies $E_1 > \langle\psi|H|\psi\rangle$, then we obtain the following lower bound:

$$E_{\text{lower}} = \langle\psi|H|\psi\rangle - \frac{\sigma^2}{E_1 - \langle\psi|H|\psi\rangle}, \tag{3}$$

where $\sigma = \sqrt{\langle\psi|H^2|\psi\rangle - \langle\psi|H|\psi\rangle^2}$.

This inequality requires precise knowledge of E_1. However, for many practical applications, it is difficult to determine the exact value of the first-excited-state energy. Thus we consider a case for which we know an approximate (or a lower-bounded) value of the first-excited-state energy. In this case, we can use the following inequality.

Theorem 3. If the state $|\psi\rangle$ and the approximate first-excited-state energy E_1^{app} satisfy $E_1 > E_1^{\text{app}} > \langle\psi|H|\psi\rangle$, then we obtain the following lower bound:

$$E_{\text{lower}} = \langle\psi|H|\psi\rangle - \frac{\sigma^2}{E_1^{\text{app}} - \langle\psi|H|\psi\rangle}, \tag{4}$$

where $\sigma = \sqrt{\langle\psi|H^2|\psi\rangle - \langle\psi|H|\psi\rangle^2}$.

IV. METHOD

Here, we present our scheme for estimating a ground-state energy with guaranteed accuracy for QA in a certain condition. We use the two inequalities presented in the previous section to obtain the error bars for QA.

To use these inequalities, we must measure the expectation value and standard deviation of the Hamiltonian after QA. In practice, the quantum states become mixed states because the nondiagonal terms in the density matrix decay owing to decoherence. After implementing QA, we measure only the Hamiltonian and standard deviation. In this case, we can show that the nondiagonal terms in the energy basis do not affect the expectation value and standard deviation of the Hamiltonian. Hence we can describe the quantum state after QA as either a pure state or a mixed state as long as the energy population between them is the same. For simplicity, we use a pure state for the description.

Suppose that we obtain a state of $|\phi_0^{(\text{ann})}\rangle$ after QA. We rewrite this state as follows:

$$\left|\phi_0^{(\text{ann})}\right\rangle = \sqrt{1-\epsilon^2}\,|\phi_0\rangle + \sum_{m\neq 0} \epsilon_m\,|\phi_m\rangle\,, \tag{5}$$

where $|\phi_0\rangle$ denotes the ground state, $|\phi_m\rangle$ $(m > 0)$ denotes the mth excited state, ϵ_m denotes the amplitude of the mth excited state, and ϵ denotes the amplitude of all the states except the ground state. In other words, $\sqrt{1-\epsilon^2}$ denotes the amplitude of the ground state. Owing to normalization, we have a condition $\epsilon^2 = \sum_{m\neq 0} \epsilon_m^2$. As we consider the expectation value of the Hamiltonian and the standard deviation, the relative phase between the energy eigenstates does not affect our results. Therefore, we can assume ϵ_m to be real values without loss of generality throughout this paper. The squared standard deviation ΔE^2 is given by

$$\Delta E^2 = \left\langle \phi_0^{(\mathrm{ann})} \right| H_P^2 \left| \phi_0^{(\mathrm{ann})} \right\rangle - \left\langle \phi_0^{(\mathrm{ann})} \right| H_P \left| \phi_0^{(\mathrm{ann})} \right\rangle^2. \quad (6)$$

To quantify the accuracy of the output of QA, we define two values: an estimation error and an error bar. The estimation error is defined as

$$\delta_{\mathrm{est}} = \left\langle \phi_0^{(\mathrm{ann})} \right| H_P \left| \phi_0^{(\mathrm{ann})} \right\rangle - E_0. \quad (7)$$

It is worth mentioning that δ_{est} is always positive because E_0 provides the lowest energy. However, it is difficult to measure the estimation error experimentally. Therefore, we define an error bar $\delta_{\mathrm{errorbar}}$ as the upper bound of the estimation error, such as $\delta_{\mathrm{est}} < \delta_{\mathrm{errorbar}}$, and the objective of our study is to present a method for determining the error bar from experimentally observable quantities.

A. Bounds on the error of the energy using the Weinstein bound for QA

First, we explain how to use the Weinstein bound to obtain the error bar from experimentally observable quantities.

By applying the Weinstein bound to the case of QA, we can rewrite Theorem 1 in the following form.

Theorem 4. If $\epsilon^2 \leqslant \frac{1}{2}$ is satisfied, then

$$\Delta E^2 - \left(\langle \phi_0^{(\mathrm{ann})} | H_P | \phi_0^{(\mathrm{ann})} \rangle - \langle \phi_0 | H_P | \phi_0 \rangle \right)^2 \geqslant 0. \quad (8)$$

Thus we regard the standard deviation as the error bar and the lower bound of the ground-state energy is given by $\langle \phi_0^{(\mathrm{ann})} | H_P | \phi_0^{(\mathrm{ann})} \rangle - \Delta E$. However, if we only use experimental results with QA, it is not straightforward to judge whether the condition $\frac{1}{2} \geqslant \epsilon^2$ is satisfied.

We present a method for judging whether $\frac{1}{2} \geqslant \epsilon^2$ is satisfied. The key idea is to combine QA with classical computation. In particular, we perform a preestimation of the energies of the ground state and first excited state. We can employ a classical computer for such a preestimation by using a suitable approximation, such as a mean-field technique or variational methods. Let $\tilde{E}_0$ ($\tilde{E}_1$) denote the approximate value of the ground (first-excited) -state energy calculated from the preestimation. If this preestimation is sufficiently accurate, the condition $\frac{1}{2} \geqslant \epsilon^2$ is satisfied; hence we can use the standard deviation of the energy to obtain the upper bound of the error estimation, as will be explained later.

There are many ways to calculate the ground-state and excited-state energies of molecules in quantum chemistry using a classical computer. For example, a variational trial function gives us the upper bound of the ground-state energy. In addition, there is a way to estimate the lower bound of the ground-state energy [69]. Furthermore, various ways to obtain the energy gap between the ground state and the excited states are known [70–73]. By combining these techniques, the range of the ground-state and first-excited-state energies can be obtained.

The classical estimation error between the approximate energy $\tilde{E}_n$ and the true energy E_n is denoted by $\delta\tilde{E}_n$. Thus we have the equality

$$\tilde{E}_n = E_n + \delta\tilde{E}_n. \quad (9)$$

We assume that the classical estimation errors are bounded as follows:

$$|\delta\tilde{E}_0| < \delta M_0, \quad |\delta\tilde{E}_1| < \delta M_1, \quad (10)$$

where δM_0 and δM_1 denote the classical error bars representing the accuracy of the preestimation. We assume that both δM_0 and δM_1 are positive. We can show that the sufficient condition of the inequality $\frac{1}{2} \geqslant \epsilon^2$ is

$$E_0^{(\mathrm{ann})} \leqslant \tfrac{1}{2}(E_0 + E_1), \quad (11)$$

where $E_0^{(\mathrm{ann})} = \langle \phi_0^{(\mathrm{ann})} | H_P | \phi_0^{(\mathrm{ann})} \rangle$ is the energy of the state $|\phi_0^{(\mathrm{ann})}\rangle$. Substituting (9) into (11), we obtain

$$(E_0 <) E_0^{(\mathrm{ann})} < \tfrac{1}{2}(\tilde{E}_0 + \tilde{E}_1) - \tfrac{1}{2}(\delta\tilde{E}_0 + \delta\tilde{E}_1). \quad (12)$$

We obtain a sufficient condition for (12) as follows:

$$(E_0 <) E_0^{(\mathrm{ann})} < \tfrac{1}{2}(\tilde{E}_0 + \tilde{E}_1) - \tfrac{1}{2}(|\delta\tilde{E}_0| + |\delta\tilde{E}_1|). \quad (13)$$

From $|\delta\tilde{E}_0| < \delta M_0$ and $|\delta\tilde{E}_1| < \delta M_1$, a sufficient condition for (13) is

$$(E_0 <) E_0^{(\mathrm{ann})} < \tfrac{1}{2}(\tilde{E}_0 + \tilde{E}_1) - \tfrac{1}{2}(\delta M_0 + \delta M_1). \quad (14)$$

From the approximate energy by the preestimation ($\tilde{E}_0$ and $\tilde{E}_1$) and the upper bound of the classical estimation errors (δM_0 and δM_1), Eq. (14) is the sufficient condition of (11). This means that, as long as (14) is satisfied, we can use the standard deviation of the energy as the new error bar (corresponding to the upper bound of the estimation error) of the energy estimation. In particular, when the new error bar given by the standard deviation is smaller than δM_0, the ground-state energy estimated by QA is closer to the ground-state energy than the preestimation.

Note that the condition given by (14) is not always satisfied. If there are significant effects of decoherence and/or nonadiabatic transitions, $E_0^{(\mathrm{ann})}$ may be large such that the sufficient condition is not satisfied. Alternatively, if the estimation error $(\delta M_0 + \delta M_1)$ is large, again, it becomes more difficult to satisfy the sufficient condition. For example, at least, $(\delta M_0 + \delta M_1)$ should be sufficiently small to satisfy the following conditions:

$$E_0 < \tfrac{1}{2}(\tilde{E}_0 + \tilde{E}_1) - \tfrac{1}{2}(\delta M_0 + \delta M_1). \quad (15)$$

Otherwise, we cannot use the Weinstein bound regardless of the results of QA. In these cases, we should try other approaches, such as optimizing the QA schedule, fabricating new samples with lower decoherence, or more precise preestimation with a longer calculation time using a classical computer to satisfy the condition given by (14).

B. Bounds on the error of the energy using the Temple bound for QA

Second, we explain how to use the Temple bound to obtain the error bar from experimentally observable quantities. By applying Theorem 2 to the case of QA, we obtain the following.

Theorem 5. If the condition $E_1 > \langle\phi_0^{(\mathrm{ann})}| H |\phi_0^{(\mathrm{ann})}\rangle$ is satisfied, then we obtain the lower bound of the ground-state energy:

$$E_{\mathrm{lower}}^{T} = \langle\phi^{(\mathrm{ann})}| H |\phi^{(\mathrm{ann})}\rangle - \frac{\Delta E^2}{E_1 - \langle\phi^{(\mathrm{ann})}| H |\phi^{(\mathrm{ann})}\rangle}, \quad (16)$$

where E_1 is the exact energy for the first excited state.

However, to use this inequality, we need to determine the exact value of the first-excited-state energy, which is difficult using a classical computer. Therefore, we consider replacing the exact first-excited-state energy E_1 with an approximate value. By applying Theorem 3 to our case, we obtain the following form.

Theorem 6. If the approximate first-excited-state energy $E_1^{(\mathrm{low})}$ satisfies $E_1 > E_1^{(\mathrm{low})} > \langle H\rangle$, then we obtain the lower bound

$$E_{\mathrm{lower}}^{T'} = \langle\phi^{(\mathrm{ann})}| H |\phi^{(\mathrm{ann})}\rangle - \frac{\Delta E^2}{E_1^{(\mathrm{low})} - \langle\phi^{(\mathrm{ann})}| H |\phi^{(\mathrm{ann})}\rangle}. \quad (17)$$

We show how the Temple bound can be used for QA by preestimation of the energy via classical computation. We need to determine the lower bound of the excited-state energy. Hence, similar to the case of the Weinstein bound, we assume that $\tilde{E}_1 = E_1 + \delta\tilde{E}_1$ with $|\delta\tilde{E}_1| < \delta M_1$ from classical computation. In this case, we set $E_1^{(\mathrm{low})} = \tilde{E}_1 - \delta M_1$. Suppose that we obtain $E_0^{(\mathrm{ann})}$ after performing QA. If $E_0^{(\mathrm{ann})} < E_1^{(\mathrm{low})}$ is satisfied, we can use the Temple bound to obtain the lower bound of the ground-state energy, which corresponds to the error bar of the QA estimation.

C. Comparison between the Weinstein bound and the Temple bound

Here, we explain how to compare the error bars obtained from the Weinstein bound with those obtained from the Temple bound when we perform QA. It is worth mentioning that the performance strongly depends on the accuracy of the preestimation; hence the comparison is not straightforward. In particular, the Weinstein bound requires preestimation of both the ground state and the first excited state, whereas the Temple bound requires preestimation of only the first excited state. Moreover, the accuracy of the Temple bound depends on how accurately we can estimate the first-excited-state energy, whereas the accuracy of the Weinstein bound does not depend on the accuracy of the preestimation as long as the condition described in (14) is satisfied.

We consider the following two extreme cases for the comparison; the Temple bound is advantageous in one of them and disadvantageous in the other. First, by assuming that we have perfect knowledge of the first excited state, we set $E_1^{(\mathrm{low})} = E_1$. In this case, the Temple bound is advantageous. Second, we assume that we have the least knowledge of the first excited state under the constraint that (15) is satisfied. This corresponds to the worst case of the Temple bound, while we can still employ the Weinstein bound if we use long-lived qubits with QA. More specifically, by substituting $\tilde{E}_0 = E_0$ into (15), we obtain $\delta M_1 < \tilde{E}_1 - E_0$. By assuming that $\tilde{E}_1 = E_1 - \delta M_1$, we obtain the lower bound of the first-excited-state energy $\tilde{E}_1 > \frac{E_0+E_1}{2}$. From these calculations, we choose $E_1^{(\mathrm{low})} = \frac{E_0+E_1}{2}$. In this case, the Temple bound is disadvantageous. In Sec. V, when we compare the Temple bound with the Weinstein bound, we consider these two conditions.

D. Measurement of the energy and standard deviation of the Hamiltonian

We describe how to measure the energy and standard deviation of the Hamiltonian in QA. We assume that we can perform any single-qubit measurements in QA. The Hamiltonian is now written in the form $H = \sum_j \hat{P}_j$, where $\hat{P}_j$ denotes the product of the Pauli matrices (such as $\hat{\sigma}_0^z, \hat{\sigma}_1^z, \ldots$ and $\hat{\sigma}_0^x\hat{\sigma}_1^x\hat{\sigma}_2^y\hat{\sigma}_3^y$). After the preparation of the ground state with QA, we can implement single-qubit measurements to obtain $\langle\hat{P}_1\rangle$. This means that, by repeating the experiments (that involve the ground-state preparation and single-qubit measurements), we can measure $\langle\hat{P}_j\rangle$ for every j and obtain $\langle H\rangle$ by summing them up. Similarly, we can measure $\langle H^2\rangle$; hence we can also measure the standard deviation of the energy. These techniques have been used in the algorithms of NISQ devices [18,74].

We explain a possible experimental implementation for measuring the energy and standard deviation of the Hamiltonian. In conventional QA, we cannot perform arbitary single-qubit operations. For example, in the current D-Wave machine, the available operations are adiabatic changes of external fields and measurements of $\hat{\sigma}_z$. In this case, it is not possible to measure the standard deviation of the energy because of the requirement to measure $\hat{\sigma}_x$ and $\hat{\sigma}_y$. However, owing to recent developments in QA from both theoretical and experimental aspects, such measurements would be available for cutting-edge devices. A capacitively shunted flux qubit (CSFQ) is another candidate for realizing QA with a long coherence time [75,76]. The CSFQ was originally developed for a gate-type quantum computer and arbitrary single-qubit operations can be implemented on it with microwave pulses [75,76]. Recently, there was a theoretical proposal for using this device in QA [40]; hence single-qubit operations are available with the CSFQ during QA. More details about this method are described in Appendix D. Therefore, CSFQs are suitable for our scheme owing to the ability of the arbitrary single-qubit operations.

V. NUMERICAL RESULTS

This section describes numerical simulations performed to obtain the error of the energy estimated using our method. In particular, we consider the hydrogen molecule. The Hamiltonian of the hydrogen molecule can be described by the Pauli matrices. To consider the decoherence, we simulate QA with the Lindblad master equation and discuss the relation between the decoherence rate and the accuracy of the energy estimation. In addition, we plot the improved error bars obtained from our methods.

TABLE I. Coefficient of the hydrogen molecule. The unit of these values is GHz, as described in the main text.

h_0	−0.09706626816762881
h_1	0.17141282644776895
h_2	0.16868898170361213
h_3	−0.22343153690813586
h_4	0.17441287612261597
h_5	0.12062523483390428
h_6	0.17141282644776892
h_7	0.04530261550379928
h_8	0.04530261550379928
h_9	0.16592785033770355
h_{10}	−0.22343153690813589
h_{11}	0.12062523483390428
h_{12}	0.04530261550379928
h_{13}	0.04530261550379928
h_{14}	0.16592785033770355

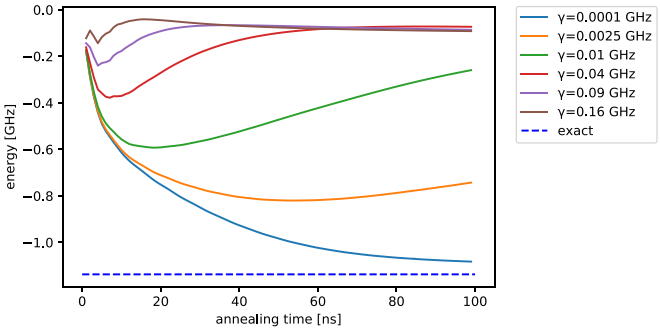

FIG. 3. Plots showing the relation between the annealing time and the ground-state energy by QA. We consider the hydrogen molecule with an interatomic distance of 0.74 Å. The vertical axis represents the energy, while the horizontal axis represents the annealing time T for each decoherence rate γ. Values of γ from top to bottom in legend correlate with solid curves in the figure from bottom to top.

We introduce the Lindblad master equation. We consider the time-dependent system Hamiltonian $H(t)$ under a noisy environment. The Lindblad master equation that we use in this paper is given by

$$\frac{d\rho(t)}{dt} = -i[H(t), \rho(t)] + \sum_n \gamma\left[\sigma_n^{(k)}\rho(t)\sigma_n^{(k)} - \rho(t)\right], \tag{18}$$

where $\sigma_j^{(k)}(k = x, y, z)$ denotes the Pauli matrix acting at site j, γ denotes the decoherence rate, and $\rho(t)$ is the density matrix of the quantum state at time t. We solve the Lindblad master equation numerically using QuTiP [77,78]. Throughout this paper, we choose the decoherence type σ_j^z as the Lindblad operator. This type of noise has been investigated in a previous study to consider the effect of noise on the superconducting qubits [79].

The Hamiltonian of the hydrogen molecule is given by

$$\begin{aligned} H = {} & h_0 I + h_1\hat{\sigma}_0^z + h_2\hat{\sigma}_1^z + h_3\hat{\sigma}_2^z + h_4\hat{\sigma}_1^z\hat{\sigma}_3^z \\ & + h_5\hat{\sigma}_0^z\hat{\sigma}_2^z + h_6\hat{\sigma}_0^z\hat{\sigma}_1^z + h_7\hat{\sigma}_0^x\hat{\sigma}_1^z\hat{\sigma}_2^x + h_8\hat{\sigma}_0^y\hat{\sigma}_1^z\hat{\sigma}_2^y \\ & + h_9\hat{\sigma}_0^z\hat{\sigma}_1^z\hat{\sigma}_2^z + h_{10}\hat{\sigma}_1^z\hat{\sigma}_2^z\hat{\sigma}_3^z + h_{11}\hat{\sigma}_0^z\hat{\sigma}_2^z\hat{\sigma}_3^z \\ & + h_{12}\hat{\sigma}_0^x\hat{\sigma}_1^z\hat{\sigma}_2^x\hat{\sigma}_3^z + h_{13}\hat{\sigma}_0^y\hat{\sigma}_1^z\hat{\sigma}_2^y\hat{\sigma}_3^z + h_{14}\hat{\sigma}_0^z\hat{\sigma}_1^z\hat{\sigma}_2^z\hat{\sigma}_3^z, \end{aligned} \tag{19}$$

where we have used STO-3G basis and Bravyi–Kitaev transformation. The coefficients of the Hamiltonian (19), $h_0, \ldots, h_{14}$, depend on the interatomic distance. We assume that the interatomic distance is 0.74 Å. The coefficient of the Hamiltonian (19) corresponding to the above-mentioned interatomic distance is listed in Table I and it is calculated using OpenFermion [80].

The most promising device for QA is a superconducting qubit. We mainly consider the implementation of superconducting qubits. The typical energy scale of the superconducting qubit is of the order of GHz [81]. Therefore, we adopt this energy scale to describe the Hamiltonian.

The relation between the measured energy and the annealing time is shown in Fig. 3. We can choose the annealing time to minimize the energy of the problem Hamiltonian after QA. Throughout this paper, we choose such an optimized annealing time for the plots. Importantly, as the decoherence rate increases, the minimum energy after the optimization increases because the decoherence can induce a transition from the ground state to the excited states.

By applying the method described in Sec. IV A, we numerically determine the conditions that satisfy $\frac{1}{2} \geqslant \epsilon^2$ with the preestimation when we estimate the ground-state energy of the hydrogen molecule. In other words, we show the region where we can use the Weinstein bound so that we can use the standard deviation as the upper bound of the estimation error. Such a region is plotted in Fig. 4(a). Moreover, for the case of $E_1^{(\mathrm{low})} = (E_0 + E_1)/2$, we can also use the Temple bound in this region. As the decoherence rate increases, preestimation should be performed more precisely to satisfy $\frac{1}{2} \geqslant \epsilon^2$. Meanwhile, even when we can use the standard deviation obtained from QA as the new error bound (owing to the satisfaction of the condition $\frac{1}{2} \geqslant \epsilon^2$), the preestimation could still provide a closer to ground-state energy than the QA if the standard deviation is larger. We plot the condition when the standard deviation is smaller than δM_0 while the condition $\frac{1}{2} \geqslant \epsilon^2$ is satisfied, as shown in Fig. 4(b).

In Fig. 5, we plot the estimation of the ground-state energy and the lower bound obtained by the Weinstein and Temple bounds when we use our scheme in QA. As the decoherence rate decreases, the error bar (providing the lower bound of the ground state) becomes smaller.

In Fig. 6, we show how close the estimation error corresponding to the Weinstein and Temple bounds is to the chemical accuracy [here, we assume that either $E_1^{(\mathrm{low})} = E_1$ or $E_1^{(\mathrm{low})} = (E_0 + E_1)/2$ when we use the Temple bound, as explained in Sec. IV C]. Furthermore, for comparison, we show the chemical accuracy of the hydrogen molecule. When the decoherence rate is lower than 10^{-5}, the energy measured using the Temple bound is within the chemical accuracy.

In this section, we calculate the error bars for the energy obtained by QA for a Hamiltonian written in qubits obtained by the Bravyi–Kitaev transformation of molecular hydrogen. Meanwhile, in Appendix C, we calculate the error bars for the energy obtained by QA for the Jordan–Wigner transformation of molecular hydrogen and obtain similar results. In addition,

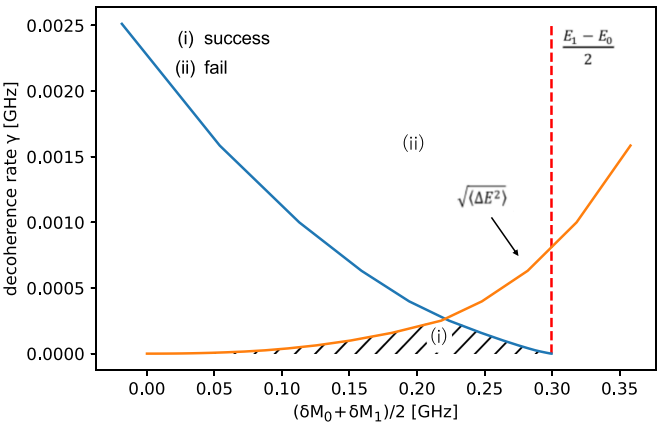

FIG. 4. Plot of two types of threshold decoherence rate. One of them is for the Weinstein bound to be applied. The other one is for our scheme using the Weinstein bound to be more precise than the preestimation using a classical computer. As long as the decoherence rate of QA is lower than the threshold (blue line in the plot), we can apply the Weinstein bound; hence the standard deviation can be the upper bound of the estimation error of QA. If $(\delta M_0 + \delta M_1)/2$ becomes equal to or larger than $(E_1 - E_0)/2$, our protocol always fails regardless of the value of the decoherence rate. As long as the decoherence rate of QA is lower than the threshold (orange line in the plot), the standard deviation given from our scheme is more precise upper bound than the preestimation error of QA. For simplicity, we assume that $\frac{1}{2}(\tilde{E}_0 + \tilde{E}_1) = \frac{1}{2}(E_0 + E_1)$ in these plots. Here, we say that our scheme succeeds when we can apply the Weinstein bound based on this prescription and the ground-state energy estimated by QA is closer to the ground-state energy than the preestimation.

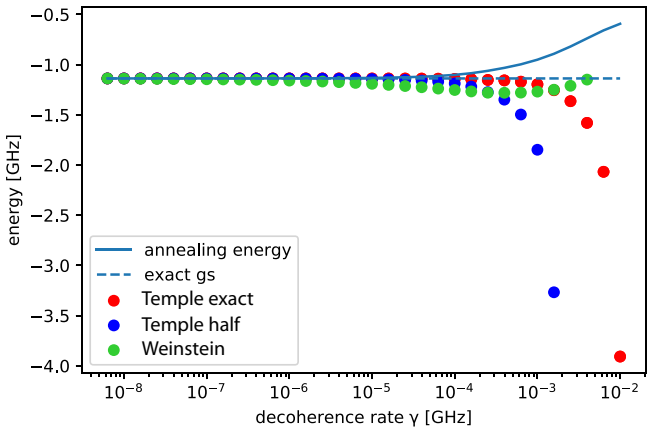

FIG. 5. We plot the energy expectation value with the lower bound (calculated from the error bars) of the ground-state energy in our scheme. The dashed line represents the exact ground-state energy. The solid line represents the energy expectation value $(E_0^{(\mathrm{ann})})$ obtained from QA. The green dots represent the lower bound obtained from the Weinstein bound. The red dots represent the lower bound obtained from the Temple bound when $E_1^{(\mathrm{low})}$ in (17) is the exact first-excited-state energy E_1. The blue dots represent the lower bound obtained from the Temple bound when $E_1^{(\mathrm{low})}$ in (17) is $(E_0 + E_1)/2$.

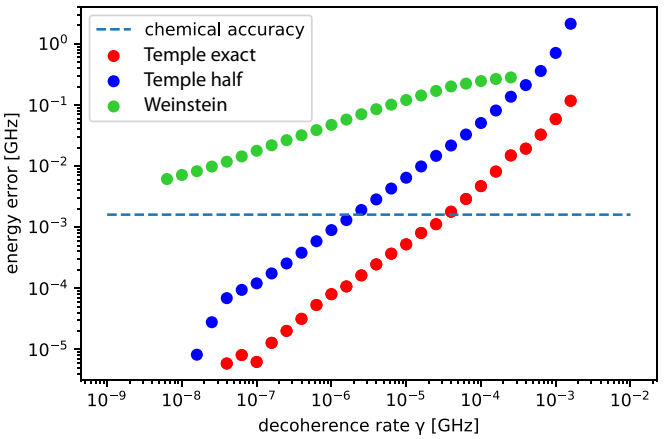

FIG. 6. We plot the estimation error and chemical accuracy (dotted line) against the decoherence rate. The green dots represent the lower bound obtained from the Weinstein bound. The red dots represent the lower bound obtained from the Temple bound when $E_1^{(\mathrm{low})}$ in (17) is the exact first-excited-state energy E_1. The blue dots represent the lower bound obtained from the Temple bound when $E_1^{(\mathrm{low})}$ in (17) is $(E_0 + E_1)/2$.

we verify that our scheme can be applied to the case of lithium hydride, as explained in Appendix A.

VI. CONCLUSION

In this paper, we proposed a method for estimating the energy of the target Hamiltonian with improved accuracy by combining QA with classical computation. Based on the Weinstein bound, if the population of the ground state is more than $1/2$ after QA, the error of the energy for the problem Hamiltonian is upper bounded by the standard deviation. To check whether the population of the ground state is more than $1/2$ after QA, we used classical computation for the preestimation of the energy of the ground state and first excited state. More precisely, we obtained the approximate energy of the problem Hamiltonian with possible error bars for the ground state and first excited state by performing classical computation with some approximation (such as a mean-field technique). From the values obtained by the preestimation, we can calculate a threshold; if the energy of the state after QA is lower than the threshold, the population of the ground state is more than $1/2$ after QA. In addition, if the standard deviation of QA is smaller than the error bar in the preestimation, we can use the standard deviation as the improved error bar. Moreover, to obtain a further improved error bar, we employed the Temple bound for QA. In this case, it is necessary to determine the lower bound of the energy of the first excited state using classical computation. If the estimation of the ground-state energy with QA is lower than the bound, we can obtain the error bar of the estimation. We numerically showed that the error bar obtained from the Temple bound provides a better bound than that obtained from the Weinstein bound. Our methods are useful for improving the accuracy of quantum chemistry calculations, especially when QA with long-lived qubits is realized experimentally.

Finally, we discuss the scope for future work. Recently, variationally scheduled quantum simulation has been pro-

posed, where annealing scheduling has been optimized to minimize the expectation value of the Hamiltonian [82–88]. In this case, for the optimization of the scheduling parameters, it is necessary to iterate QA many times. However, in this scheme, there is no information about the estimation error of the energy. By combining this method with our proposal, the expectation value of the Hamiltonian can be decreased and the accuracy can be improved via measurement of the standard deviation, because the decrease in the expectation value of the Hamiltonian usually decreases the energy error of the Temple and Weinstein bounds when the system is close to the ground state. Further research is required to quantify the performance of such a hybrid strategy, and we leave this as a topic for future study.

ACKNOWLEDGMENTS

We are grateful for the insightful discussions with K. Sugisaki and H. Katsura. This work was supported by the Leading Initiative for Excellent Young Researchers, MEXT Japan, and JST PRESTO (Grant No. JPMJPR1919), Japan. This paper is partly based on the results obtained from a project, No. JPNP16007, commissioned by the New Energy and Industrial Technology Development Organization (NEDO), Japan.

APPENDIX A: LITHIUM HYDRIDE MOLECULE

In this section, we describe the application of our scheme to the lithium hydride molecule. The Hamiltonian of the lithium hydride molecule is given by the spin systems, where we use the STO-3G basis and Jordan–Wigner transformation. We set the interatomic distance to 2.04 Å. The coefficients of the Hamiltonian depend on the interatomic distance. We obtain the coefficients using OpenFermion [80]. As there are 12 qubits in this system, the computational cost is too high to consider the decoherence by solving the Lindblad master equation. Therefore, we use the time-dependent Schrödinger equation without decoherence in our calculations. We set the annealing time from 10^2 ns to 10^5 ns. In Fig. 7, we plot the energy expectation value obtained by annealing with error bars obtained by measuring the energy standard deviation. Furthermore, we show the exact ground-state energy. In Fig. 8, we plot the estimation error and the standard deviation, where the chemical accuracy is also shown for comparison. The estimation error (the standard deviation of the energy) becomes lower than the chemical accuracy with an annealing time longer than 1.0×10^4 (5.0×10^4).

APPENDIX B: DERIVATION OF THE WEINSTEIN BOUND FOR QA

In this section, we derive the Weinstein bound (Theorem 4). First, we explain the estimation error and standard deviation.

The estimation error of the energy eigenvalue of the problem Hamiltonian is given by

$$\langle\phi|\, H_P\, |\phi\rangle - \langle\phi_0|\, H_P\, |\phi_0\rangle = \sum_{m\neq 0} \epsilon_m^2 (E_m - E_0), \tag{B1}$$

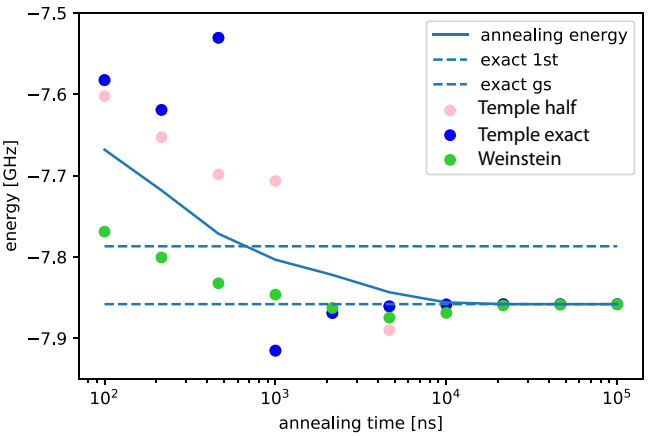

FIG. 7. Energy expectation value with the error bar in our scheme. The solid line represents the energy expectation value ($E_0^{(\mathrm{ann})}$) obtained from QA. The dashed line represents the exact ground-state and first-excited-state energies. The green dots represent the lower bound obtained from the Weinstein bound. The red dots represent the lower bound obtained from the Temple bound when $E_1^{(\mathrm{low})}$ in (17) is the exact first-excited-state energy E_1. The blue dots represent the lower bound obtained from the Temple bound when $E_1^{(\mathrm{low})}$ in (17) is $(E_0 + E_1)/2$.

where H_P is the problem Hamiltonian, E_m is the mth energy eigenvalue of the problem Hamiltonian, and $|\phi\rangle$ is the state that satisfies $\langle\phi|\phi_0\rangle \geqslant \frac{1}{2}$. Meanwhile, the squared standard deviation ΔE^2 is given by

$$\begin{aligned}\Delta E^2 &= \langle\phi|\, H_P^2\, |\phi\rangle - \langle\phi|\, H_P\, |\phi\rangle^2 \\ &= \sum_{m\neq 0} \epsilon_m^2 (E_m - E_0)^2 - \left(\sum_{m\neq 0} \epsilon_m^2 (E_m - E_0)\right)^2. \end{aligned} \tag{B2}$$

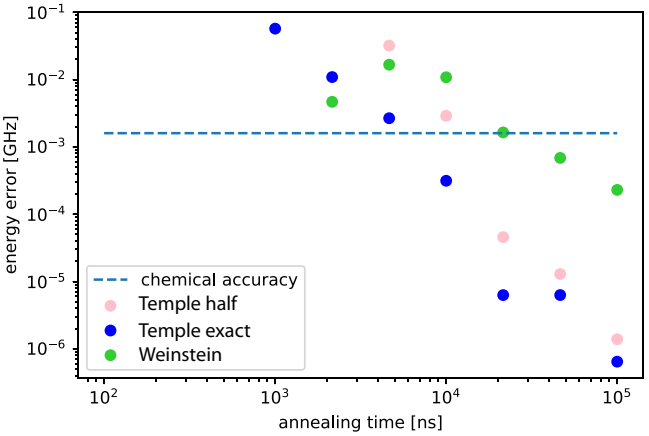

FIG. 8. We plot the estimation error and the chemical accuracy (dotted line) against the decoherence rate. The green dots represent the lower bound obtained from the Weinstein bound. The red dots represent the lower bound obtained from the Temple bound when $E_1^{(\mathrm{low})}$ in (17) is the exact first-excited-state energy E_1. The blue dots represent the lower bound obtained from the Temple bound when $E_1^{(\mathrm{low})}$ in (17) is $(E_0 + E_1)/2$.

We subtract the squared error of the energy from the energy dispersion ΔE^2 as follows:

$$\Delta E^2 - (\langle\phi| H_P |\phi\rangle - \langle\phi_0| H_P |\phi_0\rangle)^2 = \sum_{m\neq 0} \epsilon_m^2 (E_m - E_0)^2 - 2\left(\sum_{m\neq 0} \epsilon_m^2 (E_m - E_0)\right)^2. \quad \text{(B3)}$$

We consider the relation between the standard deviation and the estimation error of the energy eigenvalue. We remark that the following inequality holds from the Cauchy–Schwarz inequality:

$$\left(\sum_{m\neq n} \epsilon_m^2 (E_m - E_n)\right)^2 \leqslant \left(\sum_{m\neq n} \epsilon_m^2\right)\left(\sum_{m\neq n} \epsilon_m^2 (E_m - E_n)^2\right). \quad \text{(B4)}$$

The lower bound of the difference between the squared standard deviation and the squared error of the energy (B3) is given as follows:

$$\begin{aligned}
&\Delta E^2 - (\langle\phi| H_P |\phi\rangle - \langle\phi_0| H_P |\phi_0\rangle)^2 \\
&= \sum_{m\neq 0} \epsilon_m^2 (E_m - E_0)^2 - 2\left(\sum_{m\neq 0} \epsilon_m^2 (E_m - E_0)\right)^2 \\
&\geqslant \sum_{m\neq 0} \epsilon_m^2 (E_m - E_0)^2 - 2\epsilon^2 \sum_{m\neq 0} \epsilon_m^2 (E_m - E_0)^2 \\
&= (1 - 2\epsilon^2) \sum_{m\neq 0} \epsilon_m^2 (E_m - E_0)^2, \quad \text{(B5)}
\end{aligned}$$

where we have used (B4) to rewrite the inequality. Finally, from $\sum_{m\neq 0} \epsilon_m^2 (E_m - E_0)^2 \geqslant 0$ in the equations above, the proof of Theorem 4 is complete.

APPENDIX C: HYDROGEN MOLECULE OF JORDAN–WIGNER TRANSFORMATION

In this section, we discuss the case of using the Jordan–Wigner transformation. First, in this case, the Hamiltonian of the hydrogen molecule is given by

$$\begin{aligned}
H = {} & h_0 I + h_1 \hat{\sigma}_0^z + h_2 \hat{\sigma}_1^z + h_3 \hat{\sigma}_2^z + h_4 \hat{\sigma}_3^z \\
& + h_5 \hat{\sigma}_0^z \hat{\sigma}_1^z + h_6 \hat{\sigma}_0^z \hat{\sigma}_2^z + h_7 \hat{\sigma}_1^z \hat{\sigma}_2^z + h_8 \hat{\sigma}_0^z \hat{\sigma}_3^z + h_9 \hat{\sigma}_1^z \hat{\sigma}_3^z \\
& + h_{10} \hat{\sigma}_2^z \hat{\sigma}_3^z + h_{11} \hat{\sigma}_0^y \hat{\sigma}_1^y \hat{\sigma}_2^x \hat{\sigma}_3^x + h_{12} \hat{\sigma}_0^x \hat{\sigma}_1^y \hat{\sigma}_2^y \hat{\sigma}_3^x \\
& + h_{13} \hat{\sigma}_0^y \hat{\sigma}_1^x \hat{\sigma}_2^x \hat{\sigma}_3^y + h_{14} \hat{\sigma}_0^x \hat{\sigma}_1^x \hat{\sigma}_2^y \hat{\sigma}_3^y, \quad \text{(C1)}
\end{aligned}$$

where we have used the STO-3G basis. The coefficient of this Hamiltonian is listed in Table II.

We plot the relation between the annealing time and the energy after QA in Fig. 9. This is nearly identical to Fig. 3.

We plot the lower bound of the energy and the error of the energy using our method for the Jordan–Wigner and Bravyi–Kitaev transformations in Fig. 10 and Fig. 11. We can see that the results of the Jordan–Wigner transformation are slightly more accurate than those of the Bravyi–Kitaev transformation.

TABLE II. Coefficient of the hydrogen molecule using the Jordan–Wigner transformation. The unit of these values is GHz, as described in the main text.

h_0	−0.09706626816762881
h_1	0.17141282644776895
h_2	0.17141282644776892
h_3	−0.22343153690813586
h_4	−0.22343153690813589
h_5	0.16868898170361213
h_6	0.12062523483390428
h_7	0.16592785033770355
h_8	0.16592785033770355
h_9	0.12062523483390428
h_{10}	0.17441287612261597
h_{11}	−0.04530261550379928
h_{12}	0.04530261550379928
h_{13}	0.04530261550379928
h_{14}	−0.04530261550379928

APPENDIX D: POSSIBLE EXPERIMENTAL IMPLEMENTATION OF SINGLE QUBIT OPERATIONS IN QA BY USING CSFQ

In this section, we show how to realize the single qubit operation in QA by using CSFQs. It is worth mentioning that, by combining single-qubit measurements in the computational basis and single-qubit rotations, it is possible to implement single-qubit measurements in an arbitrary basis. This section is divided into two parts. The first one is a review of spin-lock techniques for QA by using CSFQ. The second one is to explain how single-qubit operation can be performed in QA by using the spin-lock techniques.

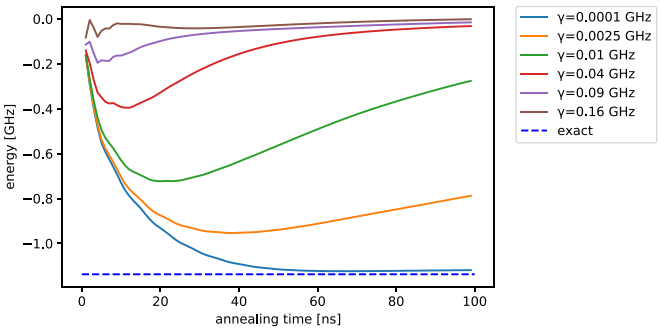

FIG. 9. Plots showing the relation between the annealing time and the ground-state energy by QA. We consider the hydrogen molecule with an interatomic distance of 0.74 Å. The vertical axis represents the energy, while the horizontal axis represents the annealing time T for each decoherence rate γ. Values of γ from top to bottom in legend correlate with solid curves in the figure from bottom to top.

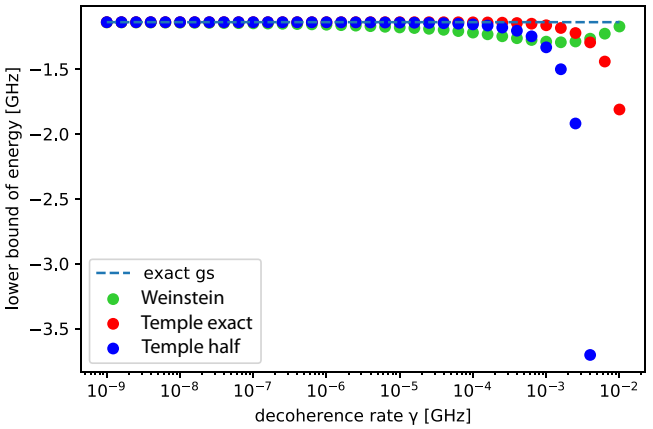

FIG. 10. We plot the energy expectation value with the lower bound of the ground-state energy in our scheme. The dashed line represents the exact ground-state energy. The green dots represent the lower bound obtained from the Weinstein bound. The red dots represent the lower bound obtained from the Temple bound when a in (17) is the exact first-excited-state energy E_1. The blue dots represent the lower bound obtained from the Temple bound when a in (17) is $(E_0 + E_1)/2$. This case corresponds to the worst case of the preestimation.

1. Spin-lock quantum annealing

In this subsection, we explain about the spin-lock QA [40]. This is a method to realize quantum annealing in CSFQ with a microwave driving field. Suppose that we drive inductively coupled CSFQs with a microwave field. In this case, the Hamiltonian during QA (before the readout) is given by

$$H(t) = \sum_j \frac{w}{2}\hat{\sigma}_j^z + \lambda(t)\hat{\sigma}_j^x \cos wt + g(t)H_P, \tag{D1}$$

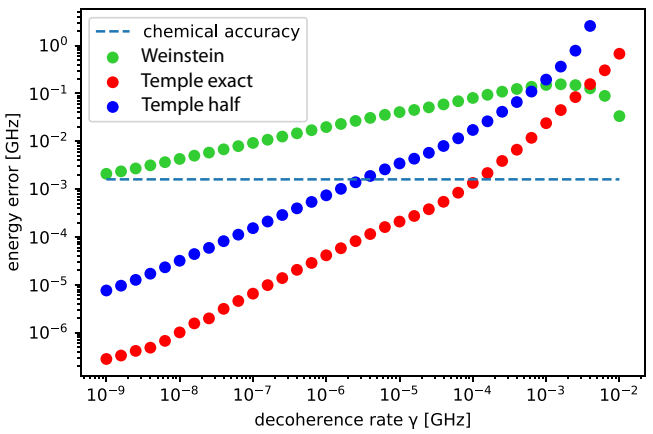

FIG. 11. We plot the estimation error and chemical accuracy (dotted line) against the decoherence rate. The green dots represent the lower bound obtained from the Weinstein bound. The red dots represent the lower bound obtained from the Temple bound when a in (17) is the exact first-excited-state energy E_1. The blue dots represent the lower bound obtained from the Temple bound when a in (17) is $(E_0 + E_1)/2$. This case corresponds to the worst case of the preestimation.

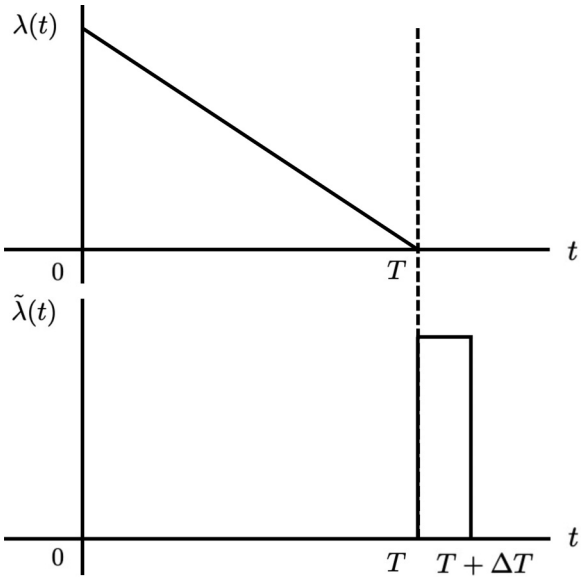

FIG. 12. Schedule of parameters $\lambda(t)$ and $\tilde{\lambda}(t)$.

where $\lambda(t) = (1 - \frac{t}{T})\lambda_0$ denotes a time-dependent driving amplitude, $g(t) = \frac{t}{T}$ denotes a scheduling of the coupling strength, and H_P denotes the problem Hamiltonian. We assume that H_P commutes with $\sum_j \hat{\sigma}_j^z$ and actually the problem Hamiltonians adopted in our paper satisfy these properties. By going to a rotating frame, the Hamiltonian is rewritten as

$$\hat{H} = UHU^\dagger - iU^\dagger \frac{dU}{dt}, \tag{D2}$$

where U is a unitary operator to denote the rotating frame. In this section, we choose the following:

$$U = \exp\left(-it\sum_{j=1}^{L}\frac{w}{2}\hat{\sigma}_j^z\right). \tag{D3}$$

By using the rotating wave approximation, we obtain the following Hamiltonian:

$$\hat{H}(t) = \sum_j \lambda(t)\hat{\sigma}_j^x + g(t)H_P \tag{D4}$$

and this is the same Hamiltonian that we use in the main text.

2. Realizing the single qubit operation

In this subsection, we explain how to realize single qubit rotations. After the evolution with the Hamiltonian in the Eq. (D4), we have

$$H(t = T) = \sum_j \frac{w}{2}\hat{\sigma}_j^z + H_P \tag{D5}$$

at $t = T$. We apply microwave pulses and the Hamiltonian is given as

$$H(t = T + \tau) = \sum_j \frac{w}{2}\hat{\sigma}_j^z + \tilde{\lambda}(t)\hat{\sigma}_j^x \cos(w'\tau + \theta) + H_P, \tag{D6}$$

where $\tilde{\lambda}(t)$ denotes the time-dependent amplitude of the driving fields (see Fig. 12):

$$\tilde{\lambda}(t) = \begin{cases} \tilde{\lambda}, & T \leqslant t \leqslant T + \Delta T, \\ 0, & \text{otherwise.} \end{cases} \tag{D7}$$

Equation (D6) in the rotating frame is given by

$$\hat{H}(t) = \sum_j \left(\frac{w - w'}{2} \hat{\sigma}_j^z + \tilde{\lambda}(t) \cos\theta \hat{\sigma}_j^x + \tilde{\lambda}(t) \sin\theta \hat{\sigma}_j^y \right) + H_P \tag{D8}$$

using the unitary operator

$$U' = \exp\left(-it \sum_{j=1}^{L} \frac{w'}{2} \hat{\sigma}_j^z \right). \tag{D9}$$

When the magnitude of the driving fields is much larger than any coefficient of the problem Hamiltonian, we obtain the following Hamiltonian in a rotating frame:

$$\hat{H}(t) \simeq \sum_j \left(\frac{w - w'}{2} \hat{\sigma}_j^z + \tilde{\lambda}(t) \cos\theta \hat{\sigma}_j^x + \tilde{\lambda}(t) \sin\theta \hat{\sigma}_j^y \right). \tag{D10}$$

This means that we can realize arbitrary single qubit rotations with the CSFQ. By combining this with a single qubit measurement in the computational basis, we can realize single qubit measurements in an arbitrary basis.

[1] H. Eyring, J. Chem. Phys. **3**, 107 (1935).
[2] S. B. Bravyi and A. Y. Kitaev, Ann. Phys. (NY) **298**, 210 (2002).
[3] F. Verstraete and J. I. Cirac, J. Stat. Mech.: Theory Exp. (2005) P09012.
[4] J. T. Seeley, M. J. Richard, and P. J. Love, J. Chem. Phys. **137**, 224109 (2012).
[5] A. Tranter, S. Sofia, J. Seeley, M. Kaicher, J. McClean, R. Babbush, P. V. Coveney, F. Mintert, F. Wilhelm, and P. J. Love, Int. J. Quantum Chem. **115**, 1431 (2015).
[6] R. Xia, T. Bian, and S. Kais, J. Phys. Chem. B **122**, 3384 (2018).
[7] J. D. Biamonte and P. J. Love, Phys. Rev. A **78**, 012352 (2008).
[8] W. Lechner, P. Hauke, and P. Zoller, Sci. Adv. **1**, e1500838 (2015).
[9] A. Tranter, P. J. Love, F. Mintert, and P. V. Coveney, J. Chem. Theory Comput. **14**, 5617 (2018).
[10] R. Babbush, P. J. Love, and A. Aspuru-Guzik, Sci. Rep. **4**, 6603 (2015).
[11] T. Takeshita, N. C. Rubin, Z. Jiang, E. Lee, R. Babbush, and J. R. McClean, Phys. Rev. X **10**, 011004 (2020).
[12] L. Mueck, Nat. Chem. **7**, 361 (2015).
[13] R. Babbush, N. Wiebe, J. McClean, J. McClain, H. Neven, and G. K.-L. Chan, Phys. Rev. X **8**, 011044 (2018).
[14] A. Aspuru-Guzik, A. D. Dutoi, P. J. Love, and M. Head-Gordon, Science **309**, 1704 (2005).
[15] J. D. Whitfield, J. Biamonte, and A. Aspuru-Guzik, Mol. Phys. **109**, 735 (2011).
[16] F. Arute, K. Arya, R. Babbush, D. Bacon, J. C. Bardin, R. Barends, R. Biswas, S. Boixo, F. G. Brandao, D. A. Buell *et al.*, Nature (London) **574**, 505 (2019).
[17] D.-B. Zhang, Z.-H. Yuan, and T. Yin, arXiv:2006.15781.
[18] S. Endo, Z. Cai, S. C. Benjamin, and X. Yuan, J. Phys. Soc. Jpn. **90**, 032001 (2021).
[19] A. Peruzzo, J. McClean, P. Shadbolt, M.-H. Yung, X.-Q. Zhou, P. J. Love, A. Aspuru-Guzik, and J. L. O'brien, Nat. Commun. **5**, 4213 (2014).
[20] J. R. McClean, J. Romero, R. Babbush, and A. Aspuru-Guzik, New J. Phys. **18**, 023023 (2016).
[21] Y. Li and S. C. Benjamin, Phys. Rev. X **7**, 021050 (2017).
[22] M.-C. Chen, M. Gong, X. Xu, X. Yuan, J.-W. Wang, C. Wang, C. Ying, J. Lin, Y. Xu, Y. Wu *et al.*, Phys. Rev. Lett. **125**, 180501 (2020).
[23] A. Kardashin, A. Uvarov, D. Yudin, and J. Biamonte, Phys. Rev. A **102**, 052610 (2020).
[24] T. Kadowaki and H. Nishimori, Phys. Rev. E **58**, 5355 (1998).
[25] Y. Matsuzaki, H. Hakoshima, K. Sugisaki, Y. Seki, and S. Kawabata, Jpn. J. Appl. Phys. **60**, SBBI02 (2021).
[26] J. Copenhaver, A. Wasserman, and B. Wehefritz-Kaufmann, J. Chem. Phys. **154**, 034105 (2021).
[27] G. Mazzola, V. N. Smelyanskiy, and M. Troyer, Phys. Rev. B **96**, 134305 (2017).
[28] S. N. Genin, I. G. Ryabinkin, and A. F. Izmaylov, arXiv:1901.04715.
[29] M. Streif, F. Neukart, and M. Leib, *Solving Quantum Chemistry Problems with a d-Wave Quantum Annealer* (Springer, New York, 2019).
[30] A. Teplukhin, B. K. Kendrick, and D. Babikov, J. Chem. Theory Comput. **15**, 4555 (2019).
[31] Y. Seki, Y. Matsuzaki, and S. Kawabata, Bull. Am. Phys. Soc. **65** (2020).
[32] M. W. Johnson, M. H. Amin, S. Gildert, T. Lanting, F. Hamze, N. Dickson, R. Harris, A. J. Berkley, J. Johansson, P. Bunyk *et al.*, Nature (London) **473**, 194 (2011).
[33] K. Kudo, Phys. Rev. A **98**, 022301 (2018).
[34] S. H. Adachi and M. P. Henderson, arXiv:1510.06356.
[35] F. Hu, B.-N. Wang, N. Wang, and C. Wang, Quantum Eng. **1**, e12 (2019).
[36] K. Kudo, J. Phys. Soc. Jpn. **89**, 064001 (2020).
[37] I. Ozfidan, C. Deng, A. Smirnov, T. Lanting, R. Harris, L. Swenson, J. Whittaker, F. Altomare, M. Babcock, C. Baron *et al.*, Phys. Rev. Appl. **13**, 034037 (2020).
[38] W. Vinci and D. A. Lidar, npj Quantum Inf. **3**, 38 (2017).
[39] A. D. King, S. Suzuki, J. Raymond, A. Zucca, T. Lanting, F. Altomare, A. J. Berkley, S. Ejtemaee, E. Hoskinson, S. Huang *et al.*, arXiv:2202.05847.
[40] Y. Matsuzaki, H. Hakoshima, Y. Seki, and S. Kawabata, Jpn. J. Appl. Phys. **59**, SGGI06 (2020).
[41] T. Imoto, Y. Seki, and Y. Matsuzaki, J. Phys. Soc. Jpn. **91**, 064004 (2022).

[42] Y. Seki and H. Nishimori, Phys. Rev. E **85**, 051112 (2012).
[43] Y. Seki and H. Nishimori, J. Phys. A: Math. Theor. **48**, 335301 (2015).
[44] V. Choi, arXiv:2105.02110.
[45] H. Nishimori and K. Takada, Front. ICT **4**, 2 (2017).
[46] Y. Susa, Y. Yamashiro, M. Yamamoto, and H. Nishimori, J. Phys. Soc. Jpn. **87**, 023002 (2018).
[47] Y. Susa, Y. Yamashiro, M. Yamamoto, I. Hen, D. A. Lidar, and H. Nishimori, Phys. Rev. A **98**, 042326 (2018).
[48] K. L. Pudenz, T. Albash, and D. A. Lidar, Nat. Commun. **5**, 3243 (2014).
[49] H. Chen, X. Kong, B. Chong, G. Qin, X. Zhou, X. Peng, and J. Du, Phys. Rev. A **83**, 032314 (2011).
[50] M. Nakahara, *Lectures on Quantum Computing, Thermodynamics and Statistical Physics* (World Scientific, Singapore, 2013).
[51] T. Albash and D. A. Lidar, Phys. Rev. A **91**, 062320 (2015).
[52] T. Suzuki and H. Nakazato, arXiv:2006.13440.
[53] E. Crosson, E. Farhi, C. Y.-Y. Lin, H.-H. Lin, and P. Shor, arXiv:1401.7320.
[54] H. Goto and T. Kanao, Commun. Phys. **3**, 235 (2020).
[55] L. Hormozi, E. W. Brown, G. Carleo, and M. Troyer, Phys. Rev. B **95**, 184416 (2017).
[56] S. Muthukrishnan, T. Albash, and D. A. Lidar, Phys. Rev. X **6**, 031010 (2016).
[57] L. T. Brady and W. van Dam, Phys. Rev. A **95**, 032335 (2017).
[58] R. D. Somma, D. Nagaj, and M. Kieferová, Phys. Rev. Lett. **109**, 050501 (2012).
[59] A. Das and B. K. Chakrabarti, Rev. Mod. Phys. **80**, 1061 (2008).
[60] V. Karanikolas and S. Kawabata, J. Phys. Soc. Jpn. **89**, 094003 (2020).
[61] K. Funo, N. Lambert, and F. Nori, Phys. Rev. Lett. **127**, 150401 (2021).
[62] L. Prielinger, A. Hartmann, Y. Yamashiro, K. Nishimura, W. Lechner, and H. Nishimori, Phys. Rev. Res. **3**, 013227 (2021).
[63] K. Funo, J.-N. Zhang, C. Chatou, K. Kim, M. Ueda, and A. del Campo, Phys. Rev. Lett. **118**, 100602 (2017).
[64] G. Vacanti, R. Fazio, S. Montangero, G. Palma, M. Paternostro, and V. Vedral, New J. Phys. **16**, 053017 (2014).
[65] A. C. Santos and M. S. Sarandy, Phys. Rev. A **104**, 062421 (2021).
[66] A. Hartmann, G. B. Mbeng, and W. Lechner, Phys. Rev. A **105**, 022614 (2022).
[67] G. Passarelli, R. Fazio, and P. Lucignano, Phys. Rev. A **105**, 022618 (2022).
[68] D. Weinstein, Proc. Natl. Acad. Sci. USA **20**, 529 (1934).
[69] G. Temple, Proc. R. Soc. London, Ser. A, Containing Papers Math. Phys. Character **119**, 276 (1928).
[70] P.-F. Loos, A. Scemama, and D. Jacquemin, J. Phys. Chem. Lett. **11**, 2374 (2020).
[71] H. Nakatsuji, Bull. Chem. Soc. Jpn. **78**, 1705 (2005).
[72] Z.-L. Cai and J. R. Reimers, J. Phys. Chem. A **104**, 8389 (2000).
[73] M. R. Silva-Junior, M. Schreiber, S. P. Sauer, and W. Thiel, J. Chem. Phys. **129**, 104103 (2008).
[74] M. Cerezo, A. Arrasmith, R. Babbush, S. C. Benjamin, S. Endo, K. Fujii, J. R. McClean, K. Mitarai, X. Yuan, L. Cincio *et al.*, Nat. Rev. Phys. **3**, 625 (2021).
[75] F. Yan, S. Gustavsson, A. Kamal, J. Birenbaum, A. P. Sears, D. Hover, T. J. Gudmundsen, D. Rosenberg, G. Samach, S. Weber *et al.*, Nat. Commun. **7**, 1 (2016).
[76] L. V. Abdurakhimov, I. Mahboob, H. Toida, K. Kakuyanagi, and S. Saito, Appl. Phys. Lett. **115**, 262601 (2019).
[77] J. Johansson, Comput. Phys. Commun. **184**, 1234 (2013).
[78] J. R. Johansson, P. D. Nation, and F. Nori, Comput. Phys. Commun. **183**, 1760 (2012).
[79] S. Puri, C. K. Andersen, A. L. Grimsmo, and A. Blais, Nat. Commun. **8**, 15785 (2017).
[80] S. McArdle, S. Endo, A. Aspuru-Guzik, S. C. Benjamin, and X. Yuan, Rev. Mod. Phys. **92**, 015003 (2020).
[81] J. Clarke and F. K. Wilhelm, Nature (London) **453**, 1031 (2008).
[82] S. Matsuura, S. Buck, V. Senicourt, and A. Zaribafiyan, Phys. Rev. A **103**, 052435 (2021).
[83] Y. Susa and H. Nishimori, Phys. Rev. A **103**, 022619 (2021).
[84] H. Goto, Sci. Rep. **6**, 1 (2016).
[85] P. M. Poggi, N. K. Lysne, K. W. Kuper, I. H. Deutsch, and P. S. Jessen, PRX Quantum **1**, 020308 (2020).
[86] J. McClean, N. Rubin, K. Sung, I. D. Kivlichan, X. Bonet-Monroig, Y. Cao, C. Dai, E. S. Fried, C. Gidney, B. Gimby *et al.*, Quantum Sci. Technol. (2020).
[87] H. Goto, Phys. Rev. A **93**, 050301(R) (2016).
[88] H. Goto, J. Phys. Soc. Jpn. **88**, 061015 (2019).